Article

Characterization of a Novel Packaged Hydrogel Wound Dressing by 2.35 T Magnetic Resonance Imaging

Valentina Corradini [1], Leonardo A. Pajewski [1], Davide Di Censo [2], Marcello Alecci [2,3,4] and Angelo Galante [2,3,4,*]

1   Department of Industrial and Information Engineering and Economics, University of L'Aquila, 67100 L'Aquila, Italy
2   Department of Life, Health and Environmental Sciences, University of L'Aquila, 67100 L'Aquila, Italy
3   National Institute for Nuclear Physics (INFN), Gran Sasso National Laboratory (LNGS), 67100 L'Aquila, Italy
4   CNR-SPIN Institute, c/o Department of Physical and Chemical Sciences, 67100 L'Aquila, Italy
*   Correspondence: angelo.galante@univaq.it; Tel.: +39-0862-433495

Abstract: Hydrogel wound dressing makes easier the treatment of patients suffering from difficult wounds. A new process for the manufacturing of a sterile, packaged hydrogel wound dressing, based on an interpenetrating structure of calcium alginate, agar, and polyvinylpyrrolidone, was recently developed. The new formulation overtakes some previous technologies' drawbacks expressing a better resistance to mechanical deformations compared to products on the market. In this work, the 2.35 T proton density, spin-lattice relaxation time, spin-spin relaxation time, phase-coherence relaxation, and water apparent diffusion coefficient analysis in the new hydrogel and several alternative formulations, including a commercial one (Neoheal®), are reported. Specifically, the combination of agar, acting as a thermolabile forming agent, with calcium alginate and γ irradiated polyvinylpyrrolidone, acting, respectively, as physical, and chemical crosslinking agents with an irreversible (temperature independent) effect, have been investigated. The new hydrogel formulation brings a qualitative improvement in its handling due to its increased mechanical stiffness when compared to the commercial hydrogel reference. This comes together with a reduced water content (100 vs. 112 for proton density in arbitrary units) and swelling capacity (88% vs. 124%) but with improved water mobility (1.42 vs. 1.34×10^{-3} mm^2 s^{-1} for the apparent diffusion coefficient).

Keywords: magnetic resonance imaging; quantitative magnetic resonance imaging; hydrogel; wound dressing; calcium alginate; agar; polyvinylpyrrolidone

1. Introduction

Biocompatible nanomaterials and hydrogels are increasingly applied in the biomedical field as medical devices, including drug delivery systems, cell therapy, tissue engineering, and wound dressings [1–10].

Dressings are used for many clinical applications, such as burns, ulcers, and sores [11]. A dressing is a medical device consisting of a strip of material that may be coated on one side with an adhesive and may include a pad of surgical dressing. The dressing is used to cover and protect wounds, to support an injured part of the body, or to secure objects to the skin. A dressing is used in direct contact with a wound to help it heal and prevent further issues or complications. Different dressings are used based on the wound type, but they all aim to help reduce tissue infection. They also help with bleeding, clotting, absorption of excess fluids, and wound debridement.

The main types of dressing are generally made of pure or compound saline, pure or associated hydrocolloid, carboxymethylcellulose, pure or associated hydrophilic gel, pure or associated polyurethane films and foams, pure or associated silicone, silver associated with other substances, alginates, collagen of animal origin, and interactive composition of hyaluronic acid ester or ethyl sulfonated cellulose fibers [12]. A hydrogel is defined as a

material composed of a hydrophilic polymeric network produced by the reaction of one or more monomers, insoluble in water, and capable of retaining a significant amount of water [13]. Hydrogels find applications in various fields, such as the production of hygiene products, agriculture, drug delivery systems, pharmaceuticals, biomedical applications, tissue engineering and regenerative medicine, diagnostics, separation of biomolecules or cells, biosensors, and dressings [14–19].

Currently, two main technologies are known to produce hydrogel-based dressings used as medical devices: (i) polyvinylpyrrolidone (PVP) hydrogel, cross-linked and sterilized by irradiation [20–23]; and (ii) calcium alginate hydrogel, cross-linked by the substitution of sodium ions with calcium [24–26]. In the first case, irradiation allows both sterilization and the formation of crosslinks in the hydrogel, reducing the production timing (costs) of the biomaterial. However, the process gives a device that has the drawback of strong adhesion between the hydrogel and the final packaging case. Consequently, at the extraction time for the application, extreme care is necessary to avoid hydrogel dressing damage that could compromise its functionality. Hydrogels produced following the second method, on the other hand, do not allow sterilization by irradiation methods. Thus, hydrogel dressing must be produced starting with sterile raw materials and in a clean room, making the process cumbersome and expensive. However, alginic acid dressings have been shown to improve the healing rate and physiological mechanisms of wound repair, such as hemostasis, adhesion, and cell proliferation [27].

Magnetic Resonance Imaging (MRI) methods have been widely employed for biomaterials characterization [28–34], mapping with the sub-millimeter resolution, the spatial distribution of the relaxation times and diffusion coefficient of water contained in between compartments, pores, or biopolymer aggregates. Recently, MRI allowed controlling in a non-invasive way the survival of transplanted cells on a hydrogel matrix [35], and a wide range of hydrogel-based materials and applications [36–39] benefit from the use of this technique.

A significant body of previous work has shown several advantages of MRI for the characterization of hydrogel-based biomaterials and wound dressing, due to the non-invasive and non-destructive insight into the chemical-physical properties and safety issues as well [40]. MRI of inhomogeneous calcium alginate gel samples allowed us to successfully follow the spatial variation of alginate concentration and the distribution of pore size [28]. Moreover, MRI tracked the variation of the reaction front over the gelation process of sodium alginate by means of calcium ions [41]. It was reported that MRI is a useful tool to characterize the structures of calcium alginate gels of various compositions, thus providing an insight into the correlation between gels' chemical structure and physical properties (mechanical gel strength, porosity, and water diffusion properties). Interestingly, it was argued that the mechanical properties of hydrogels, such as the modulus of rigidity, correlates with the water transverse relaxation time [29]. Alginate hydrogel beads encapsulating cells have been used for the purpose of cell transplantation. However, their usefulness depends on the ability to maintain structural integrity for sufficient periods of time. MRI successfully monitored the temporal changes in the structure of hydrogel beads layered with poly-L-lysine over a month's culture, highlighting that this non-invasive imaging method provides valuable information about beads' integrity [31]. The biocompatibility of hydrogel-based contact lenses, known to be closely related to their oxygen permeability, was studied by means of Nuclear Magnetic Resonance (NMR), showing that the water self-diffusion coefficient is a measure of the diffusive contribution to oxygen permeability [42]. Silver-containing wound dressings are gaining more widespread use in clinical practice. 3 T MRI was used with a wide series of standard pulse sequences to assess the safe use of such dressings [43,44].

We have recently developed a new process for the manufacturing of a sterile, packaged hydrogel dressing based on an interpenetrating structure of calcium alginate, agar, and PVP [45,46]. In this work, we present the MRI characterization at 2.35 T of the new hydrogel sterile dressing. The purpose was to quantify the free water proton density (PD),

longitudinal (T_1), transverse (T_2), and phase coherence (T_2*) relaxation times, and apparent diffusion coefficient (*ADC*) of the novel hydrogel dressing, considering a commercial hydrogel (Neoheal®) as a standard reference. The measured MRI parameters were interpreted in view of the microscopic structural changes occurring in the materials under study.

2. Materials and Methods

2.1. Materials

Neoheal® was obtained from Kikgel (Lodz, Poland), and sodium alginate (catalog number 71238) from Fluka/Fisher Scientific Italia (Rodano (Mi) Italy). Dihydrate calcium chloride ($CaCl_2$*$2H_2O$) (catalog number 433381) was purchased from Carlo Erba Reagents (Cornaredo (Mi) Italy). Agar (PRS-CODEX, catalog number 141792) was purchased from Panreac AppliChem (Monza (Mb) Italy). Polyvinylpyrrolidone (Povidone Catalog BASF series Kollidon 90 F, number 81438), molecular weight-average MW = 1,000,000–1,500,000 Dalton, was purchased from BASF Fine Chemicals (Evionnaz, Switzerland SA). Polyethylene Glycol (PEG 400; PRS-CODEX, catalog number 142436) was purchased from Panreac AppliChem (Monza (Mb) Italy). F.U. grade deionized water was used for sample preparation and for swelling tests.

2.2. Novel Dressing Production Process

The novel packaged dressing production process, see Figure 1, comprises the following steps: (i) preparation, at a temperature between 70 °C and 95 °C, of an aqueous solution of agar (AG), sodium alginate (AL), and PVP; (ii) forming the solution in a cast and cooling at room temperature, to convert the solution into a thermolabile gel (i.e., susceptible to liquefaction by heating); (iii) addition of calcium ions to the thermolabile agar gel, with the formation of a body containing the crosslinked calcium alginate hydrogel (CAL), that spontaneously separates from the walls of the cast; and (iv) extraction of the body from the cast, insertion within a transparent plastic case, sealing and γ irradiation (25 kGy) to induce cross-linking of the PVP (PVPγ) and sterilize the material [45,46].
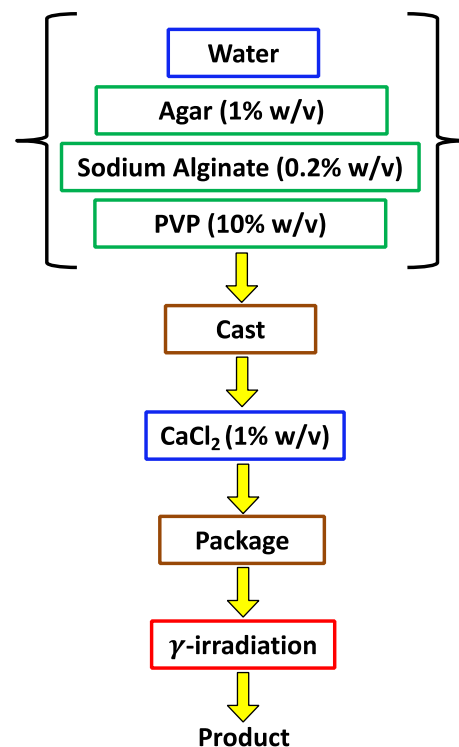

Figure 1. Schematic representation of the novel hydrogel production process [45,46].

This process, therefore, provides for a first cross-linking of sodium alginate by means of calcium ions within the aqueous solution of the thermolabile agar hydrogel, generating a volumetric retraction of the hydrogel and hence its spontaneous separation from the cast walls. Such a process further provides for a subsequent cross-linking (due to γ irradiation) of the PVP contained in the pores made by the calcium alginate hydrogel. We may suppose that the latter cross-linking occurs under high pressure due to the CAL volumetric retraction, increasing the PVP cross-linking yield and improving mechanical properties with respect to the standard hydrogel obtained by irradiating the PVP solution contained in the thermolabile agar hydrogel alone.

2.3. Hydrogel Samples Design

As reported in Table 1, in this study, we have considered six different samples to be characterized by measuring their MRI properties (PD, T_1, T_2, T_2*, ADC). Each sample was placed within a polyethylene terephthalate (PET) cast (external width 30 mm, internal width 18.5 mm; external length 47 mm, internal length 35.5 mm; depth 7.0 mm), and the effective volume of each sample was between 2 and 3 mL.

Table 1. Compositions of the hydrogel samples.

Sample	Hydrogels	Agar (% w/v)	Sodium Alginate (% w/v)	CaCl$_2$ (% w/v)	PEG (% w/v)	PVP (% w/v)	γ-Irradiation 25 kGy
S1 *	Neoheal®	1	No	No	2	10	Yes
S2	H$_2$O-AG-PEG-PVPγ	1	No	No	2	10	Yes
S3	H$_2$O-AG-PVPγ	1	No	No	No	10	Yes
S4	H$_2$O-AG-CAL	1	0.2	1	No	No	No
S5	H$_2$O-AG-CAL-PVP	1	0.2	1	No	10	No
S6	H$_2$O-AG-CAL-PVPγ	1	0.2	1	No	10	Yes

All sample preparation includes deionized water. AG = Agar; PEG = Polyethylene Glycol; PVP = Polyvinylpyrrolidone; CAL = crosslinked calcium alginate. * The Neoheal® composition is assumed from publicly available information.

All the samples (S1–S6) described in Table 1 were used to compare three different hydrogel-making procedures, where crosslinking is achieved by: the use of PVP and gamma irradiation, the use of calcium alginate, both calcium alginate and PVP gamma irradiation. S1 is the commercial hydrogel Neoheal®, taken as the reference material that implements the first hydrogel production process [20–23]. S2 has the same nominal composition as S1 but was realized in-house. It was considered both to allow a comparison with the commercial product and with S3, to quantify the presence of PEG on the MRI parameters. The composition of S4 implements the second hydrogel production process [24–26], giving insights into the combination of agar and CAL. The samples S4, S5, and S6 were selected to study the implementation steps of the novel hydrogel production process [45,46] that combines the other two methods: the effects of CAL/PVP addition and gamma irradiation. The MRI measurements were acquired in two rounds, each including four out of six samples, with the two samples undergoing repeated measurements used as a check for MRI parameters stability. The whole set of measurements allows us to compare the MRI properties of the novel hydrogel dressing, S6, with the previously known hydrogel formulations S1 and S4.

2.4. Hydrogel Samples Preparation

All samples were prepared according to the following prescriptions and heat-sealed within a casing made of a polyethylene film (case thickness comprised between 3 and 5 mm, the width of about 17 mm, length of about 33 mm, the film thickness of about 0.1 mm) before further processing (γ irradiation) and/or MRI acquisitions.

S1: Neoheal® purchased in a sealed and γ irradiated package, was cut into a plate-like strip matching the size of the other samples [20]. Its nominal composition comprises agar 1% (w/v), PVP 10% (w/v), and PEG 2% (w/v).

Agar, sodium alginate, and PVP used for the samples prepared in our laboratory were dissolved separately in warm, deionized water by continuously agitating the solutions. This dissolution stage was performed with a magnetic stirrer at (70–90 °C) for the agar and PVP and at 60 °C for the alginate, keeping the mixing for at least 60 min. Dihydrate calcium chloride was dissolved at room temperature in deionized water to a concentration of 1% (*w/v*).

S2: AG and PVP solutions were mixed, and the liquid PEG component was added in proportions such as to obtain, in the final solution, concentrations of AG, PVP, and PEG equal to 1%, 10%, and 2% (*w/v*), respectively [20]. The solution was poured into a cast and cooled at room temperature. Following the coagulation, a plate-like thermolabile gel body was formed, sealed, and irradiated.

S3: as for S2, without the PEG addiction, to obtain, in the final solution, concentrations of AG and PVP equal to 1% and 10% (*w/v*), respectively [20]. The pouring, cooling, and irradiation processes were performed as in S2.

S4: the AG and sodium alginate solutions were well mixed such as to obtain, in the final solution, concentrations of 1% and 0.2% (*w/v*), respectively [24]. The mixture was placed into an oven for 3 h at 80 °C until cleared from air bubbles, then poured into a flattened inner cavity of a cast and cooled at room temperature. Following the coagulation, a plate-like thermolabile gel body was formed, which was dipped in the aqueous calcium chloride solution previously prepared. The diffusion of calcium ions within the agar hydrogel leads to the formation of calcium alginate and agar hydrogel with a slight volumetric retraction. At the end of this crosslinking process, we observed the detachment of the hydrogel plate from the cast walls. This hydrogel plate was then heat-sealed.

S5 and S6: The AG and sodium alginate solution were prepared as in S4, adding hot PVP to reach a final concentration of 0.2%, 1%, and 10% (*w/v*), respectively [45,46]. The preparation then proceeded as in S4 with the final irradiation for S6 only, thus producing the cross-linking of PVP and the new sterile hydrogel.

Figure 2 shows the extraction of the commercial S1 and novel S6 hydrogels from the production cases. For S1, a rigid cast is mandatory to provide the hydrogel shape during gamma irradiation. The S6 instead takes its shape with the alginate crosslinking process, and then it can be extracted and sealed in the final package before undergoing irradiation. It can be noted the elastic stress on S1 is due to detachment from the container, while S6 is easily extracted from the case.
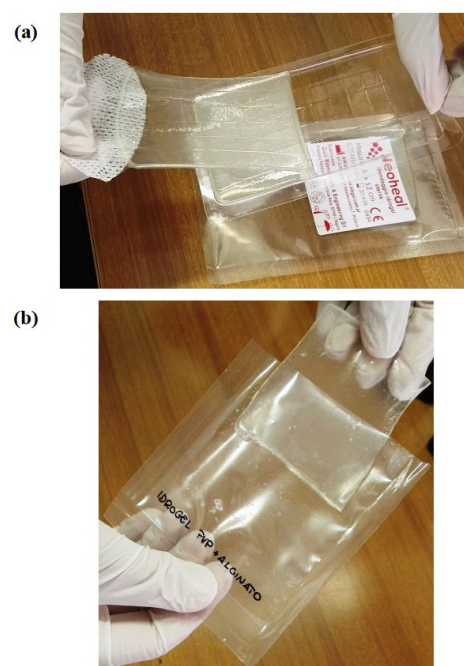

Figure 2. Extraction of the commercial (**a**) and novel (**b**) hydrogels.

2.5. Gamma Irradiation

Gamma irradiation of the samples S2, S3, and S6 was carried out at Gammatom S.r.l. facilities (Guanzate, Italy). A Cobalt-60 source with a total dose of 25 kGy was used.

2.6. MRI Hardware

MRI experiments were carried out with a 2.35 T Biospec scanner (Bruker, Karlsruhe, Germany) with hardware configuration previously described elsewhere [47,48]. The MRI scanner was equipped with a transmit/receive birdcage radio frequency (RF) volume coil (8 rungs, internal diameter 62 mm, external diameter 120 mm, length 111 mm; Doty Scientific Inc. Columbia, SC, USA) tuned at the proton frequency of 100.33 MHz and with impedance matching carefully adjusted such as to be at least -15 dB. The RF amplifier provided a peak power of 1 kW. The scanner was interfaced with an HP XW4600 workstation, running the Bruker Paravision 4.0 software for data acquisition.

The radio frequency coil allowed the positioning of up to four sealed samples at the same time, as shown in Figure 3. Figure 3a shows the typical sample layout used for the MRI acquisition. Axial and sagittal images see Figure 3b, were acquired for MRI quantifications.
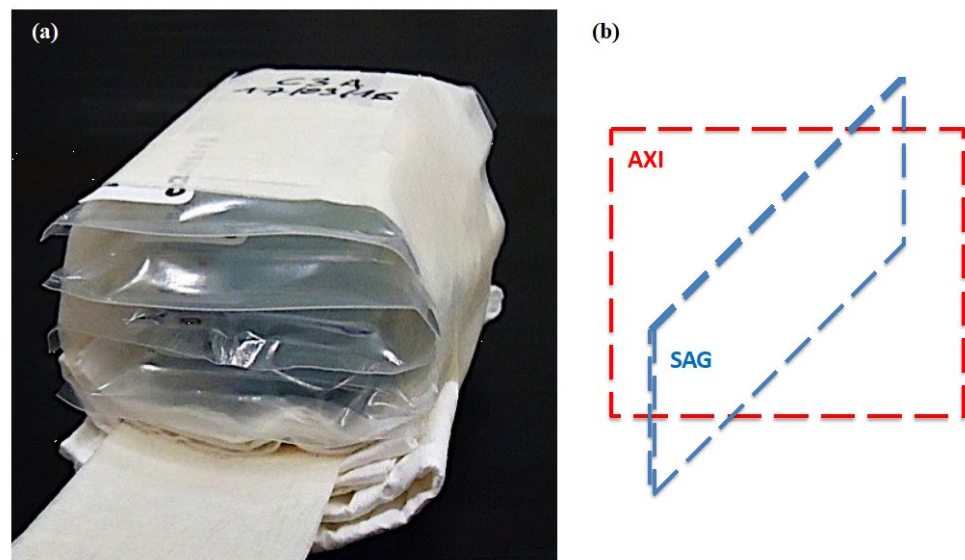

Figure 3. (**a**) Layout of an MRI phantom comprising four packaged hydrogels. (**b**) Spatial positioning of the axial and sagittal slices used for the MRI data acquisition.

2.7. MRI Acquisitions

We first applied the built-in auto-shim procedure, which reduced the NMR linewidth from about 30 to 0.5 and 2 ppm for the two phantoms under study.

Afterward, to check the position of the phantom and to obtain high spatial information about the four samples, fast gradient echo (GE) images (fast low angle shot, FLASH) [31] were acquired in the axial and sagittal planes with the following parameters: repetition time (TR) = 8000 ms; echo time (TE) = 2.9 ms; tp = 1 ms; bandwidth (BW) = 50 kHz; flip angle (FA) = 90°; Field of view (FOV) = 47 mm; 1024 × 128 pixels; spatial resolution 46 um/pixel × 367 um/pixel; slice thickness = 3 mm; the number of excitations (NEX) = 1; total acquisition time (TACQ) = 17 min. The higher spatial resolution (46 um/pixel) was selected along the anterior-posterior (AP) direction of the phantom to obtain the best spatial information along the thickness of the four samples. The ultra-short echo time (TE = 2.9 ms) was used to maximize the signal.

Axial T_1-weighted Rapid images with refocused echoes and variable repetition time (RAREVTR) [49] were acquired to map T_1 using the following parameters: TR = [16, 98, 184, 274, 370, 473, 582, 700, 826, 964, 1114, 1280, 1466, 1676, 1917, 2202, 2548, 2991, 3605, 4615, 8000] ms; TE = 10 ms; tp = 2.25 ms; BW = 43 kHz; FA = 90°; FOV = 62.8 mm × 62.8 mm; 128 × 128 pixels; spatial resolution 0.49 mm/pixel; slice thickness = 3 mm; NEX = 1; TACQ = 58 min.

An asymmetric axial T_2-weighted Multi-Slice Multi-Echo (MSME) [49] sequence was used to map T_2 using the following parameters: TR = 8000 ms; TE = k × 16 ms (k = 1, . . . , 26); tp = 5 ms; BW = 67 kHz; FA = 90°; FOV = 125.7 mm × 125.7 mm; 256 × 256 pixels; spatial resolution = 0.491 mm/pixel; 3 mm slice thickness; NEX = 1; TACQ = 26 min.

A multiple gradient echo axial T_2*-weighted sequence (MGE) [49] was used to map T_2* using the following parameters: TR = 8000 ms; TE = (3.72 + k × 4.48) ms (k = 0, . . . , 24); tp = 1.7 ms; BW = 3.1 kHz; FA = 90°; FOV = 63 × 63 mm; 128 × 128 pixels; spatial resolution 367 μm/pixel; slice thickness = 3 mm; NEX = 1; TACQ = 13 min.

ADC maps were acquired from a single axial slice 3 mm in thickness positioned in the center of the sample using a SE DtiStandard pulse sequence [49] and the following parameters: TR = 1600 ms; Teeff = 56 ms; tp = 4 ms; BW = 50 kHz; FA = 90°; diffusion gradients values b = (300, 600, 900, 1200, 1500 mm^2 s^{-1}); diffusion gradient duration and separation 22/27ms, respectively; FOV = 69.1 mm × 69.1 mm; 128 × 128 pixels; spatial resolution = 540 μm/pixel; NEX = 1; TACQ = 17 min).

1H MRS spectra were acquired using a localized Point RESolved Spectroscopy (PRESS) sequence (TR = 8000 ms; TE = 23 ms; NEX = 100; TACQ = 14 min; Time domain (TD) points = 4096; spectral width (SW) = 15 ppm) within a cubic voxel of 2.2 mm^3 without water suppression [49].

The raw images at variable TR, TE, and b values were fitted voxel-by-voxel by means of in-house developed Matlab scripts (The MathWorks, Inc., Natick, MA, USA) to obtain the *PD*, T_1, T_2, T_2* and *ADC* maps. To this purpose, the software performed 3 parameters mono-exponential fitting based on the Levenberg-Marquardt nonlinear least-squares' algorithm. From the maps, the average values in a central Region-of-Interest (ROI) comprising 3 × 3 pixels were obtained by means of the ImageJ software [50].

2.8. MRI Data Statistical Analysis

The MRI data (*PD*, T_1, T_2, T_2*, and *ADC*) were evaluated pixel by pixel. Pixels belonging to each sample were averaged after excluding pixels on the cluster's frontier to avoid partial filling effects. For each sample and MRI parameter, we also calculated the standard error of the mean (SEM). For each MRI parameter, the SEM values across the samples were stable within about 20%; we present the data with a statistical error defined as the average of the SEM among the samples.

2.9. Swelling Measurements

The swelling degree of a hydrogel can be described as its ability to absorb water. The swelling degree was calculated as a percentage: $SF(t) = 100 \times (m_t - m_0)/m_0$, where m_0 is the weight of the gel before immersion in water, and m_t is the weight at time t after immersion in water [51]. The swelling was performed by complete immersion in deionized water at room temperature, with weight measurements performed at defined time intervals.

3. Results

3.1. Quantitative MRI

Figure 4 shows high-resolution axial (a, d) and sagittal (c, f) T_2*-weighted images. We observe the presence of macroscopic air bubbles (with a diameter less than 1.5 mm) in the upper surface of samples S5 and S6, while no macroscopic air bubbles are present in the bulk of the six samples, confirming the efficacy of the preparation methods.

The axial image intensity profiles along the central lines (shown by the arrows) are reported in Figure 4b,e. They show that the slab central thickness is comprised between 3 and 5 mm and, depending on the sample composition, the signal has a single peak with a maximum at the center of the slice (S1, S3, S4) or two peaks positioned symmetrically with a minimum at the center (S2, S5, S6).
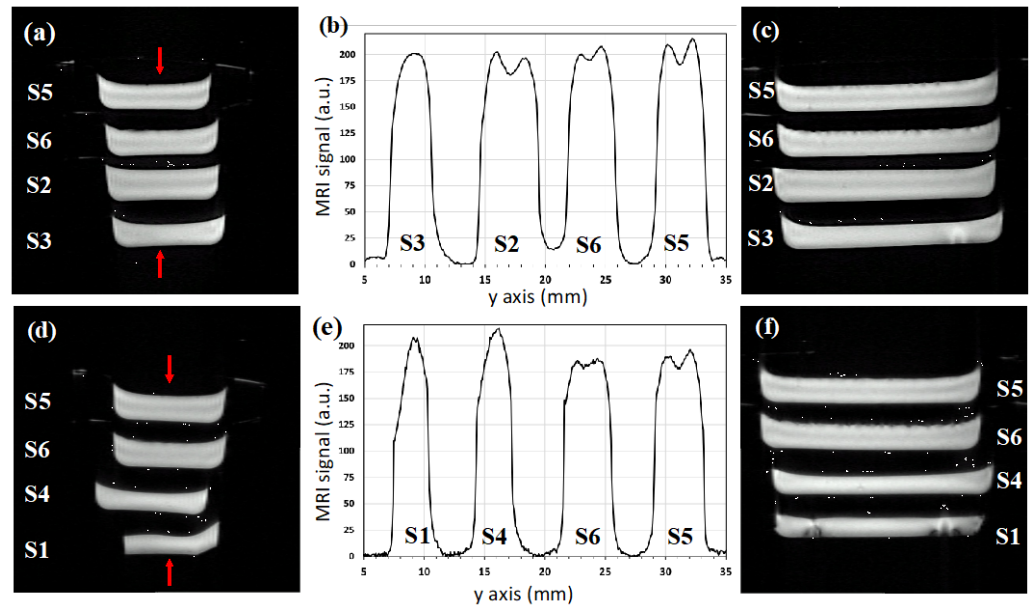
Figure 4. FLASH T_2*-weighted axial (**a**,**d**) and sagittal (**c**,**f**) images of the two MRI phantoms under study, each phantom consists of four packaged hydrogels with sample labeling and composition as in Table 1. The profiles (**b**) and (**e**) were obtained from the axial images reported, respectively, in (**a**) and (**d**), considering the central lines shown by the arrows.

Figure 5 shows the axial PD, T_1, T_2, T_2*, and ADC maps after the erosion of border voxels to avoid partial filling effects, and the average values for each sample are reported in Table 2. We observe that, depending on the hydrogel composition, the variabilities of each MRI parameter are PD from 100 to 112%; T_1 from 1320 to 2130 ms (about 47%); T_2 from 146 to 170 ms (about 15%); T_2* from 29 to 39 ms (about 29%); ADC from 1.21 to 1.67×10^{-3} mm^2 s^{-1} (about 32%).
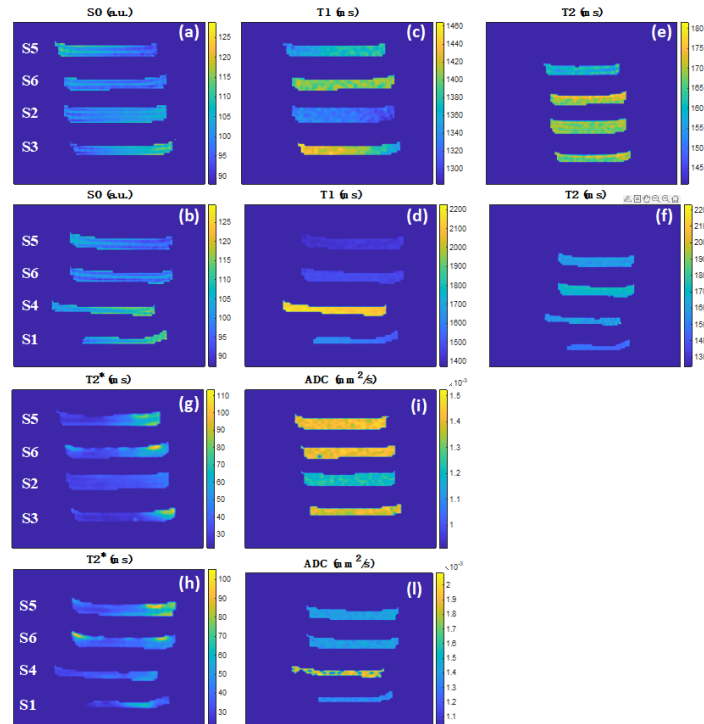

Figure 5. MRI maps from the axial acquisitions of the two MRI phantoms as from Figure 3 after edge voxels erosion. (**a**,**b**) PD in a.u., (**c**,**d**) T_1 in ms, (**e**,**f**) T_2 in ms, (**g**,**h**) T_2* in ms, and (**i**,**l**) ADC in mm^2 s^{-1}.

Table 2. Measured MRI parameters.

Sample	Hydrogels	$PD \pm 3$ (a.u.)	$T_1 \pm 30$ (ms)	$T_2 \pm 1$ (ms)	$T_2^* \pm 1$ (ms)	$ADC \pm 0.01$ ($\times 10^{-3}$ mm^2 s^{-1})
S1	Neoheal®	112	1580	146	33	1.34
S2	H$_2$O-AG-PEG-PVPγ	104	1320	168	34	1.21
S3	H$_2$O-AG-PVPγ	106	1400	169	29	1.39
S4	H$_2$O-AG-CAL	111	2130	159	37	1.67
S5	H$_2$O-AG-CAL-PVP	103	1400	160	37	1.42
S6	H$_2$O-AG-CAL-PVPγ	100	1440	170	39	1.42

From the parameters in Table 2, in the following, we compare the three hydrogel manufacturing procedures (S2, S4, S6), their intermediate steps (S3, S5), and the commercial product (S1).

For S2, the longitudinal relaxation time and the water diffusion coefficient are much lower than those reported in the literature for pure water (T_1 = 3200 ms and ADC = 2.50 × 10^{-3} mm^2 s^{-1} at room temperature [52]). The presence of the PVPγ and the thermolabile agar lattices, is capable of strongly confining the water molecules causing efficient longitudinal relaxation and reduced diffusivity.

The comparison of S2 and S3 clarifies the effect of PEG removal from the former, showing a relatively small increase in T_1 (6%) and ADC (15%) and a decrease in T_2^* (15%). In S2, we can envisage water coordination with PEG, favoring the T_1 relaxation mechanisms and reducing water diffusivity.

The comparison between S2 and S6 shows a relatively small increase in T_1 (+9%), T_2^* (+15%), and ADC (+17%). Those results seem to indicate that the replacement of the PEG polymer with the network of calcium alginate makes the longitudinal relaxation of the water molecules within the novel hydrogel matrix less efficient, i.e., reducing their dipolar interactions with the surrounding microscopic environment. The significant ADC and T_1 increase in the novel hydrogel can be interpreted as the presence of a more open lattice network that provides better conditions for water diffusion and less interaction of the water molecules with the lattice.

In S4, we observe that the T_1 and ADC are significantly lower than those of pure water. Those results can be explained by the presence of the calcium alginate lattice associated with the thermolabile agar lattice, both capable of confining the water molecules and thus shortening the longitudinal relaxation. However, the sample shows significantly larger PD (+7%), T_1 (+61%), and ADC (+38%) than S2, highlighting a more open lattice network again.

The comparison of S4 and S5, both with agar and cross-linked alginate, provides hints on the PVP effect. The latter shows a significant decrease in PD (−8%), T_1 (−34%), and ADC (−18%). As expected, the presence of PVP, a highly hydrophilic polymer, favors an efficient T_1 relaxation and reduces water diffusivity.

The comparison between S4 and S6, the latter with crosslinked PVPγ lattice shows a significant decrease in the PD (−11%), T_1 (−32%), and ADC (−15%), as expected in the presence of a less open lattice network and with values of the latter sample significantly smaller than pure water. We also observe a relatively small increase in T_2 (+7%) and T_2^* (+5%).

Samples S5 and S6 differ for the gamma-ray irradiation. The formation of intermolecular cross-links in the PVPγ gives a relatively small increase in the T_1 (+3%), T_2 (+6%) and T_2^* (+5%). We notice that the PD and ADC parameters do not change, demonstrating that they are not sensitive to the chemical crosslinking of PVPγ, although it is responsible for the formation of a mechanically stiffer lattice. Water molecules diffuse in the same way in non-cross-linked and cross-linked PVP networks, providing clues that the lattice size is not altered by gamma irradiation.

Interestingly, S6, combining the double lattice due to physical (calcium alginate) and chemical (PVPγ) crosslinking, presents T_1, T_2, and ADC values very close to the ones of S3 obtained with the chemical crosslinking alone. We conclude that the presence of physical crosslinking has no influence on these MRI parameters. Interestingly, the measurements

show that the *ADC* of S6 is about 17% larger than for S2. This can be interpreted as the presence of larger pores within the S6 lattice.

We observe differences in the MRI parameter between the novel hydrogel S6 and the commercial hydrogel S1, although a quantitative comparison is unfair since the exact composition and processing of the latter are not fully disclosed.

Figure 6 shows the PRESS spectra from a voxel localized at the center of the hydrogels S1, S4, S5, and S6. The hydrogel S1 presents a narrow symmetrical line with a bandwidth of about 0.7 ppm; S6 is an asymmetrical line with a relatively large bandwidth of about 1.5 ppm, similar to S4 (1.6 ppm) and S5 (1.4 ppm).
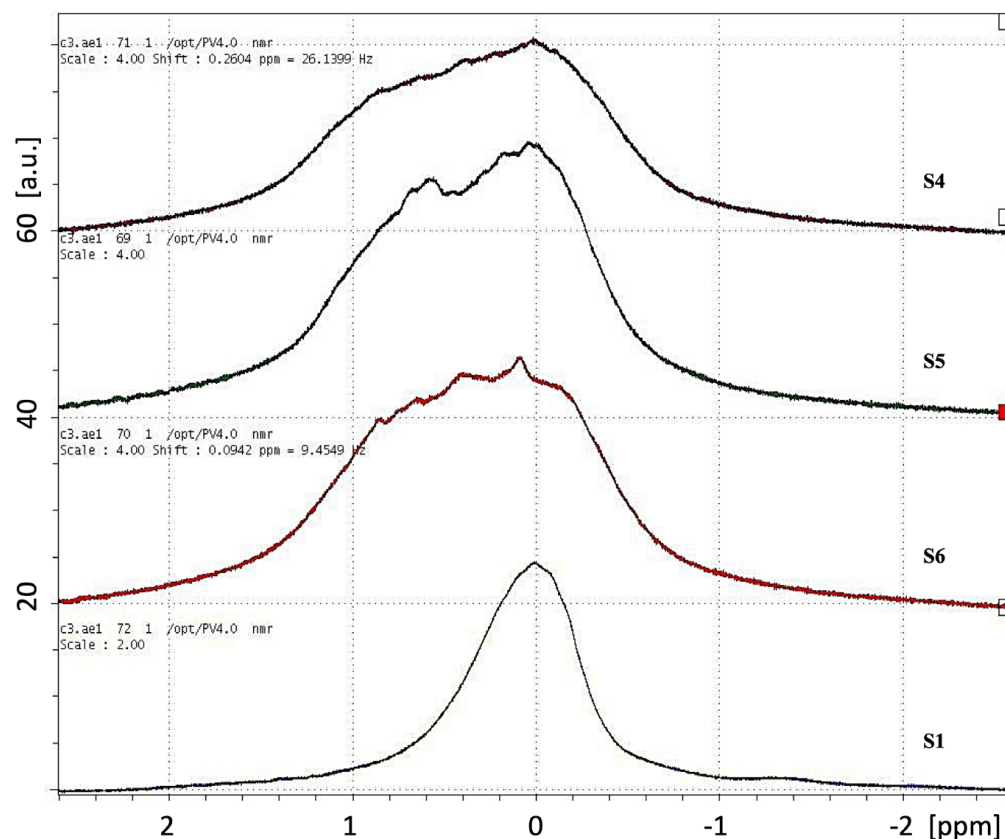

Figure 6. PRESS spectra from a small voxel (2.2 mm^3) localized at the center of the packaged hydrogels S1, S4, S5, and S6.

3.2. Swelling

Figure 7 shows the swelling degree over 100 h for samples S1, S2, and S6, representative of the chemical (S1, S2) and chemical-physical (S6) crosslinking processes. The commercial hydrogel (S1) and its laboratory replica (S2) have a large swelling capacity (up to 124% and 135%, respectively), and the difference may be due to variations in the PVP concentration, PVP being able to modulate the swelling capacity via its hydrophilicity [53].

The novel bandage (S6) has a significantly smaller swelling capacity (up to 88%) with respect to the other two samples. This can be attributed to the increased mechanical strength induced by combining PVP and calcium alginate crosslinking [54,55]. However, we have not quantified the mechanical strength of the samples, during manipulations we observed that S6 was stiffer than S2 and S1 (see Figure 2).
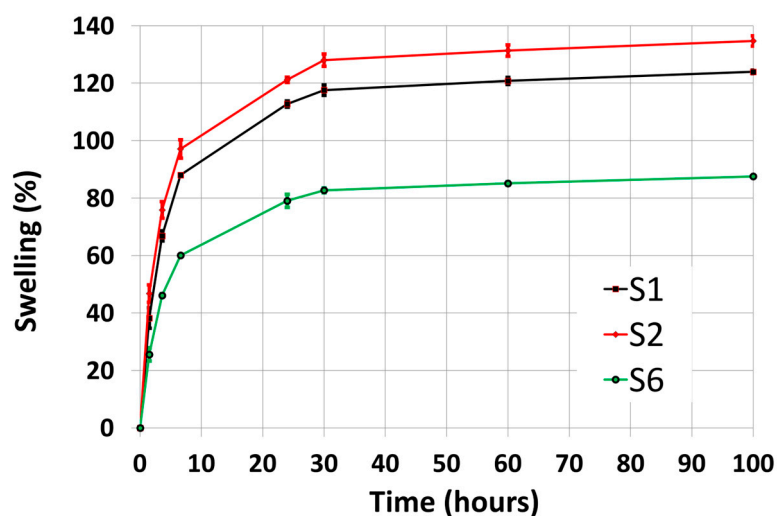
Figure 7. Swelling over 100 h of the packaged hydrogels S1, S2, and S6. Error bars are the standard error of the mean from two independent measurements.

4. Discussion

The 2.35 T MRI experimental results about proton density, spin-lattice, spin-spin, phase-coherence relaxation times, and apparent diffusion coefficient of water in the hydrogels show significant differences between the preparation procedures, allowing us to quantify different physical properties of water molecules' interactions with the lattice microscopic environment.

To the best of our knowledge, the MRI characterization of the novel hydrogel (S6) and its comparison with the previously known hydrogels (S1, S4) was not reported before. So, unfortunately, a direct comparison of our MRI results with the previous literature is not possible. In the following, we discuss the results in view of the mutual 2.35 T MRI properties between the hydrogel compositions reported in Table 2.

We have investigated the combination of agar, acting as a thermolabile forming agent, with calcium alginate and PVPγ, acting, respectively, as physical and chemical crosslinking agents, both having an irreversible (temperature independent) effect. The hydrogel preparations, combining the thermolabile forming agent with one or more irreversible crosslinking agents, give rise to a lattice able to coordinate a given amount of water. This water molecules pool with reduced mobility and very short relaxation times is not visible with the MRI instrumentation used in this work. The remaining highly mobile water molecules, providing the signal used to reconstruct the MR images, still interact among them and with the other hydrogel structures through the mechanism of dipolar spin-lattice interaction, thus defining the experimentally measured longitudinal relaxation times. The hydrogel lattice also reduces the water diffusion coefficient, with respect to pure water, due to the presence of rigid structures generated by the combination of the agar forming agent, the calcium alginate, and the PVPγ crosslinking agents. Our results show that the most sensitive MRI parameters for characterizing the hydrogels are the water spin-lattice relaxation time and diffusion coefficient.

From the localized PRESS spectra of the hydrogels S1, S4, S5, and S6 reported in Figure 6, we observe that the commercial hydrogel S1 presents a symmetrical and narrow line (0.7 ppm), while the novel hydrogel S6 shows an asymmetrical line with a relatively large bandwidth (1.5 ppm), such as the compositions S4 (1.6 ppm) and S5 (1.4 ppm). Although the limited spatial resolution of the PRESS spectra reported here, we can observe that the larger bandwidth of the samples S4, S5, and S6 are associated with their shared feature, i.e., the presence of the crosslinked calcium alginate hydrogel network. The future use of high-field NMR spectroscopy on the current hydrogel samples will allow a much better spectral resolution needed to better understand the nature of the spectral components underlying the chemical-physical properties of the hydrogel compositions [40,56–58].

In this work, we report the swelling characterization for the commercial (S1, S2) and the novel (S6) hydrogels only, representative, respectively, of the chemical and chemical-physical crosslinking processes. We found that the novel hydrogel has a lower swelling capacity and a higher diffusion coefficient with respect to the commercial hydrogel. The reduced swelling can be attributed to a significant increase in the mechanical strength due to the presence of a double crosslink mechanism (physical and chemical). Our results agree with the literature, demonstrating that an increase in hydrogel crosslinking can significantly improve mechanical strength, with a consequent reduction in the swelling capacity [54,55]. We expect that the actual swelling degree and water diffusivity of the new hydrogel may be engineered, depending on the specific application, changing the agar, PVP, and calcium alginate concentrations, but this was beyond the scope of the present work.

5. Conclusions

Our study allowed us to characterize and compare two previously known hydrogel processes [20,24] with a novel one [45,46] based on chemical and/or physical cross-linking. We observed that the commercial hydrogel [20] presents a larger water proton density and a higher swelling capacity, despite smaller water mobility and reduced mechanical properties while extracted from the package. On the contrary, the novel hydrogel [46] can retain less water and present higher water mobility and a smaller swelling degree while showing improved mechanical strength during manipulation.

We believe our quantitative MRI methodology may find useful applications in the chemical-physical characterization of a wide class of hydrogel-based wound dressing and in optimizing their industrial production processes. Moreover, the MRI hydrogel characterization reported here could find useful clinical applications in the use of hydrogels as water bolus during hyperthermia treatments for improving heat delivery [59].

Hydrogel wound dressing makes easier the treatment of patients suffering from difficult wounds, and the new formulation described here overtakes some previous technologies' drawbacks, expressing easier handling and better resistance to mechanical deformations compared to products on the market. Moreover, it should reduce vulnerability to molds [60] and have beneficial effects on the tissue repair process of wounds [61], thanks to the presence of calcium ions in the hydrogel matrix.

Finally, based on our current findings, we can envisage the following future work to better compare the standard and novel hydrogel dressing materials: microscopic characterization (SEM, TEM, AFM); mechanical tests; swelling measurements; high-resolution NMR spectroscopy.

Author Contributions: Conceptualization, L.A.P. and M.A.; methodology, V.C. and A.G.; software, D.D.C.; validation, V.C., M.A. and A.G.; investigation, M.A. and V.C.; resources, L.A.P. and A.G.; data curation, V.C., D.D.C. and A.G.; writing original draft preparation, M.A.; writing review and editing, M.A., V.C. and A.G.; visualization, D.D.C.; supervision, M.A.; project administration, A.G.; funding acquisition, L.A.P. and A.G. All authors have read and agreed to the published version of the manuscript.

Data Availability Statement: The data presented in this study are available on request from the corresponding author.

Conflicts of Interest: The authors declare no conflict of interest.

Abbreviations

The following abbreviations are used in this manuscript:

PVP	Polyvinylpyrrolidone
MRI	Magnetic Resonance Imaging
PD	Proton Density
T_1	Longitudinal relaxation times
T_2	Transverse relaxation times
T_2*	Phase-coherence relaxation times
ADC	Apparent Diffusion Coefficient
PEG	Polyethylene Glycol
PET	Polyethylene terephthalate
DSV	Diameter Spherical Volume
RF	Radio Frequency
NSPEC	Single Pulse Sequence
NMR	Nuclear Magnetic Resonance
TR	Repetition Time
tp	Pulse Length
BW	Bandwidth
NEX	Number of Excitations
TACQ	Total Acquisition Time
GE	Gradient Echo
FLASH	Fast Low Angle Shot
TE	Echo Time
FOV	Field Of View
AP	Anterior-posterior
RAREVTR	Rapid Images with Refocused Echoes and Variable Repetition Time
MSME	Multi-Slice Multi-Echo
MGE	Multiple Gradient Echo
SE	Spin Echo
b	Diffusion gradients
ROI	Region-of-Interest
SF	Swelling Degree
CAL	Crosslinked calcium alginate

References

1. Ladet, S.; David, L.; Domard, A. Multi-membrane hydrogels. *Nature* **2008**, *452*, 76–79. [CrossRef] [PubMed]
2. Hoffman, A.S. Hydrogels for biomedical applications. *Adv. Drug Deliv. Rev.* **2012**, *64*, 18–23. [CrossRef]
3. Vermonden, T.; Klumperman, B. The past, present and future of hydrogels. *Europ. Polym. J.* **2015**, *72*, 341–343. [CrossRef]
4. Naahidi, S.; Jafari, M.; Logan, M.; Wang, Y.; Yuan, Y.; Bae, H.; Dixon, B.; Chen, P. Biocompatibility of hydrogel-based scaffolds for tissue engineering applications. *Biotechnol. Adv.* **2017**, *35*, 530–544. [CrossRef] [PubMed]
5. Lee, S.H.; Shim, K.Y.; Kim, B.; Sung, J.H. Hydrogel-based three-dimensional cell culture for organ-on-a-chip applications. *Biotechnol. Prog.* **2017**, *33*, 580–589. [CrossRef] [PubMed]
6. Ivanovska, J.; Zehnder, T.; Lennert, P.; Sarker, B.; Boccaccini, A.R.; Hartmann, A.; Schneider-Stock, R.; Detsch, R. Biofabrication of 3D Alginate-Based Hydrogel for Cancer Research: Comparison of Cell Spreading, Viability, and Adhesion Characteristics of Colorectal HCT116 Tumor Cells. *Tissue Eng. Part C Methods* **2016**, *22*, 708–715. [CrossRef] [PubMed]
7. Foyt, D.A.; Norman, M.D.A.; Yu, T.T.L.; Gentleman, E. Exploiting Advanced Hydrogel Technologies to Address Key Challenges in Regenerative Medicine. *Adv. Healthcare Mater.* **2018**, *7*, 1700939. [CrossRef] [PubMed]
8. Bakker, M.H.; Tseng, C.C.S.; Keizer, H.M.; Seevinck, P.R.; Janssen, H.M.; Van Slochteren, F.J.; Chamuleau, S.A.J.; Dankers, P.Y.W. MRI Visualization of Injectable Ureidopyrimidinone Hydrogelators by Supramolecular Contrast Agent Labeling. *Adv. Healthcare Mater.* **2018**, *7*, 1701139. [CrossRef]
9. Pourshahrestani, S.; Zeimaran, E.; Kadri, N.A.; Mutlu, N.; Boccaccini, A.R. Polymeric Hydrogel Systems as Emerging Biomaterial Platforms to Enable Hemostasis and Wound Healing. *Adv. Healthcare Mater.* **2020**, *9*, 2000905. [CrossRef]
10. Tang, N.; Zheng, Y.; Cui, D.; Haick, H. Multifunctional Dressing for Wound Diagnosis and Rehabilitation. *Adv. Healthcare Mater.* **2021**, *10*, 2101292. [CrossRef]

11. Subchapter, H. (Ed.) *US Food and Drug Administration Department of Health and Human Services*; Title 21, Chapter I; Medical Devices: London, UK.

12. Commissione Regionale Dispositivi Medici (Delibera Giunta Regionale n. 1523/2008), Le Medicazioni Avanzate per il Trattamento Delle Ferite Acute e Croniche. Available online: https://salute.regione.emilia-romagna.it/normativa-e-documentazione/rapporti/dispositivi-medici/le-medicazioni-avanzate-per-il-trattamento-delle-ferite-acute-e-croniche-2016 (accessed on 20 October 2022).

13. Ahmed, E.M. Hydrogel: Preparation, characterization, and applications: A review. *J. Adv. Res.* **2015**, *6*, 105–121. [CrossRef] [PubMed]

14. Alam, P.; Shakeel, F.; Anwer, M.K.; Foudah, A.I.; Alqarni, M.H. Wound Healing Study of Eucalyptus Essential Oil Containing Nanoemulsion in Rat Model. *J. Oleo Sci.* **2018**, *67*, 957–968. [CrossRef]

15. Murakami, Y.; Fujino, T.; Kurachi, R.; Hasegawa, T.; Usui, T.; Hayase, F.; Watanabe, H. Identification of pyridinoline, a collagen crosslink, as a novel intrinsic ligand for the receptor for advanced glycation end-products (RAGE). *Biosci. Biotechnol. Biochem.* **2018**, *82*, 1508–1514. [CrossRef] [PubMed]

16. Chang, T.M.S. ARTIFICIAL CELL evolves into nanomedicine, biotherapeutics, blood substitutes, drug delivery, enzyme/gene therapy, cancer therapy, cell/stem cell therapy, nanoparticles, liposomes, bioencapsulation, replicating synthetic cells, cell encapsulation/scaffold, biosorbent/immunosorbent haemoperfusion/plasmapheresis, regenerative medicine, encapsulated microbe, nanobiotechnology, nanotechnology. *Artif. Cells Nanomed. Biotechnol.* **2019**, *47*, 997–1013. [CrossRef] [PubMed]

17. Li, Z.; Tang, M.; Dai, J.; Wang, T.; Bai, R. Effect of multiwalled carbon nanotube-grafted polymer brushes on the mechanical and swelling properties of polyacrylamide composite hydrogels. *Polymer* **2016**, *85*, 67–76. [CrossRef]

18. Li, Z.; Tang, M.; Bai, W.; Bai, R. Preparation of Hydrophilic Encapsulated Carbon Nanotubes with Polymer Brushes and Its Application in Composite Hydrogels. *Langmuir* **2017**, *33*, 6092–6101. [CrossRef] [PubMed]

19. Li, Z.; Lin, Z. Recent advances in polysaccharide-based hydrogels for synthesis and applications. *Aggregate* **2021**, *2*, e21. [CrossRef]

20. Rosiak, J.; Rucinska-Rybus, A.; Pekala, W. Method of Manufacturing Hydrogel Dressings. U.S. Patent No. 4,871,490, 30 December 1987.

21. Olejnik, A.K. Hydrogel Wound Coverings. EP1789102 B1, 9 September 2004.

22. Ajji, Z.; Othman, I.; Rosiak, J.M. Production of hydrogel wound dressings using gamma radiation. *Nucl. Instr. Meth. Phys. Res. B* **2005**, *229*, 375–380. [CrossRef]

23. Singh, R.; Singh, D. Radiation synthesis of PVP/alginate hydrogel containing nanosilver as wound dressing. *J. Mater. Sci. Mater. Med.* **2012**, *23*, 2649–2658. [CrossRef]

24. Pajewsky, L.A. Biocompatible Alginate Hydrogels. Italian Patent IT1278419, 20 November 1997.

25. Yanli, X.; Xueying, Y.; Jun, D.; Lianzhu, D.; Changlin, L.; LinJing, H.; Chunming, S. Anti-Microbial Healing-Promoting Hydrogel Dressing and Preparation Method Therefor. Chinese Patent CN103520767, 22 January 2014.

26. Lee, K.Y.; Mooney, D.J. Alginate: Properties and biomedical applications. *Progr. Polym. Sci.* **2012**, *37*, 106–126. [CrossRef]

27. Kamoun, E.A.; Kenawy, E.S.; Chen, X. A review on polymeric hydrogel membranes for wound dressing applications: PVA-based hydrogel dressings. *J. Adv. Res.* **2017**, *8*, 217–233. [CrossRef] [PubMed]

28. Potter, K.; Carpenter, T.A.; Hall, L.D. Mapping of spatial variation in alginate with calcium ions studied by magnetic resonance imaging (MRI). *Carbohydr. Res.* **1993**, *246*, 43–49. [CrossRef]

29. Degrassi, A.; Toffanin, R.; Paoletti, S.; Hall, L.D. A better understanding of the properties of alginate solutions and gels by quantitative MRI. *Carbohydr. Res.* **1998**, *306*, 19–26. [CrossRef]

30. Simpson, N.E.; Grant, S.C.; Blackband, S.J.; Constantinidis, I. NMR properties of alginate microbeads. *Biomaterials* **2003**, *24*, 4941–4948. [CrossRef]

31. Grant, S.C.; Celper, S.; Gauffin-Holmberg, I.; Simpson, N.E.; Blackband, S.J.; Constantinidis, I. Alginate assessment by NMR microscopy. *J. Mater. Sci. Mater. Med.* **2005**, *16*, 511–514. [CrossRef]

32. Bascelli, M.; Pajewski, L.A.; Fracassi, A.; Sotgiu, A.; Alecci, M. NMR Spectroscopy and Imaging of Calcium Alginate Beads Reveals Structural Heterogeneity. *Magn. Reson. Mater. Phy.* **2008**, *21*, 307–308.

33. Austin, D.T.R.; Hills, B.P. Two-dimensional NMR relaxation study of the pore structure in silicone hydrogel contact lenses. *Appl. Magn. Reson.* **2009**, *35*, 581–591. [CrossRef]

34. Iuliano, C.; Piggott, R.B.; Venturi, L.; Hills, B.P. A two-dimensional relaxation study of the evolving microstructure in a mixed biopolymer gel. *Appl. Magn. Reson.* **2010**, *38*, 307–320. [CrossRef]

35. Chan, K.W.; Liu, G.; Song, X.; Kim, H.; Yu, T.; Arifin, D.R.; Gilad, A.A.; Hanes, J.; Walczak, P.; van Zijl, P.C.; et al. MRI-detectable pH nanosensors incorporated into hydrogels for in vivo sensing of transplanted-cell viability. *Nat. Mater.* **2013**, *12*, 268–275. [CrossRef]

36. Zhao, Y.; Terai, W.; Hoshijima, Y.; Gotoh, K.; Matsuura, K.; Matsumura, K. Development and Characterization of a Poly (Vinyl Alcohol)/Graphene Oxide Composite Hydrogel as An Artificial Cartilage Material. *Appl. Sci.* **2018**, *8*, 2772. [CrossRef]

37. El-banna, F.S.; Mahfouz, M.E.; Leporatti, S.; El-Kemary, M.; Hanafy, N.A.N. Chitosan as a Natural Copolymer with Unique Properties for the Development of Hydrogels. *Appl. Sci.* **2019**, *9*, 2193. [CrossRef]

38. Patel, M.; Nakaji-Hirabayashi, T.; Matsumura, K. Effect of dual- drug- releasing micelle-hydrogel composite on wound healing in vivo in full-thickness excision wound rat model. *J. Biomed. Mat. Res. Part A* **2019**, *107*, 1094–1106. [CrossRef] [PubMed]

39. Matsumura, K. Special Issue: Nanocomposite Hydrogels for Biomedical Applications. *App. Sci.* **2020**, *10*, 389. [CrossRef]

40. Mathur, A.M.; AB Scranton, A.B. Characterization of hydrogels using nuclear magnetic resonance spectroscopy. *Biomaterials* **1996**, *17*, 547–557. [CrossRef]

41. Potter, K.; Balcom, B.J.; Carpenter, T.A.; Hall, L.D. The gelation of sodium alginate with calcium ions studied by magnetic resonance imaging (MRI). *Carbohydr. Res.* **1994**, *257*, 117–126. [CrossRef]

42. Manetti, C.; Casciani, L.; Pescosolido, N. Diffusive contribution to permeation of hydrogel contact lenses: Theoretical model and experimental evaluation by nuclear magnetic resonance techniques. *Polymer* **2002**, *43*, 87–92. [CrossRef]

43. Chaudhry, Z.; Sammet, S.; Coffey, R.; Crockett, A.; Yuh, W.T.C.; Miller, S. Assessing the safety and compatibility of silver based wound dressings in a magnetic resonance environment. *Burns* **2009**, *35*, 1080–1085. [CrossRef]

44. Bailey, J.K.; Sammet, S.; Overocker, J.; Craft-Coffman, B.; Acevedo, C.M.; Cowan, M.E.; Powell, H.M. MRI compatibility of silver based wound dressings. *Burns* **2018**, *44*, 1940–1946. [CrossRef]

45. Pajewsky, L.A.; Corradini, V.; Alecci, M. Procedimento di Produzione di un Bendaggio Idrogel Confezionato. Italian Patent N. 102016000105584, 10 April 2019.

46. Pajewsky, L.A.; Corradini, V.; Alecci, M. Process for Producing a Packaged Hydrogel Dressing. European Patent EP3311853B1, 15 July 2020.

47. Brandolini, L.; Cristiano, L.; Fidoamore, A.; De Pizzol, M.; Di Giacomo, E.; Florio, T.M.; Confalone, G.; Galante, A.; Cinque, B.; Benedetti, E.; et al. Targeting CXCR1 on breast cancer stem cells: Signaling pathways and clinical application modelling. *Oncotarget* **2015**, *6*, 43375–43394. [CrossRef]

48. Dellarosa, N.; Laghi, L.; Ragni, L.; Dalla Rosa, M.; Galante, A.; Ranieri, B.; Florio, T.M.; Alecci, M. Pulsed electric fields processing of apple tissue: Spatial distribution of electroporation by means of magnetic resonance imaging and computer vision system. *Innov. Food Sci. Emerg. Technol.* **2018**, *47*, 120–126. [CrossRef]

49. Brown, R.W.; Cheng, Y.-C.N.; Haacke, E.M.; Thompson, M.R.; Venkatesan, R. *Magnetic Resonance Imaging: Physical Principles and Sequence Design*; John Wiley & Sons: New York, NY, USA, 2014.

50. Rasband, W.S.; ImageJ. U.S. National Institutes of Health. Bethesda, Maryland, USA, 1997–2011. Available online: http://imagej.nih.gov/ij (accessed on 20 October 2022).

51. Sievers, J.; Sperlich, K.; Stahnke, T.; Kreiner, C.; Eickner, T.; Martin, H.; Guthoff, R.F.; Schünemann, M.; Bohn, S.; Stachs, O. Determination of hydrogel swelling factors by two established and a novel non-contact continuous method. *J. Appl. Polym. Sci.* **2021**, *138*, e50326. [CrossRef]

52. Wagner, F.; Laun, F.B.; Kuder, T.A.; Mlynarska, A.; Maier, F.; Faust, J.; Demberg, K.; Lindemann, L.; Rivkin, B.; Nagel, A.M.; et al. Temperature and concentration calibration of aqueous polyvinylpyrrolidone (PVP) solutions for isotropic diffusion MRI phantoms. *PLoS ONE* **2017**, *19*, e0179276. [CrossRef]

53. Baker, J.B.; Stephens, D.R.; Blanch, H.W.; Prausnitz, J.M. Swelling equilibria for acrylamide-based polyampholyte hydrogels. *Macromolecules* **1992**, *25*, 1955–1958. [CrossRef]

54. Cohen, Y.; Ramon, O.; Kopelman, I.J.; Mizrahi, S. Characterization of inhomogeneous polyacrylamide hydrogels. *J. Polym. Sci. Part B* **1992**, *30*, 1055–1067. [CrossRef]

55. Feil, H.; Bae, Y.H.; Feijen, J.; Kim, S.W. Mutual influence of pH and temperature on the swelling of ionizable and thermosensitive hydrogels. *Macromolecules* **1992**, *25*, 5528–5530. [CrossRef]

56. McConville, P.; Whittaker, M.K.; Pope, J.M. Water and Polymer Mobility in Hydrogel Biomaterials Quantified by 1H NMR: A Simple Model Describing Both T1 and T2 Relaxation. *Macromolecules* **2002**, *35*, 6961–6969. [CrossRef]

57. Lai, S.; Locci, E.; Saba, G.; Husu, I.; Masci, G.; Crescenzi, V.; Lai, A. Solid-state 13C and 129Xe NMR study of poly(vinyl alcohol) and poly(vinyl alcohol)/lactosilated chitosan gels. *J. Polym. Sci. Part A Polym. Chem.* **2003**, *41*, 3123–3131. [CrossRef]

58. Simpson, N.E.; Grant, S.C.; Gustavsson, L.; Peltronen, V.; Blackband, S.J.; Constantinidis, I. Biochemical consequences of alginate encapsulation: A NMR study of insulin secreting cells. *Biomaterials* **2006**, *27*, 2577–2586. [CrossRef]

59. Trefná, H.D.; Ström, A. Hydrogels as a water bolus during hyperthermia treatment. *Phys. Med. Biol.* **2019**, *64*, 115025. [CrossRef]

60. Goh, C.H.; Heng, P.W.; Huang, E.P.; Li, B.K.; Chan, L.W. Interactions of antimicrobial compounds with cross-linking agents of alginate dressings. *J. Antimicrob. Chemother.* **2008**, *62*, 105–108. [CrossRef]

61. Paul, W.; Sharma, C.P. Chitosan and alginate wound dressings: A short review. *Trends Biomater. Artif. Organs.* **2004**, *18*, 18–23.